

Tracing the origins of permitted emission lines in RU Lupi down to AU scales[★]

L. Podio¹, P. J. V. Garcia^{2,3}, F. Bacciotti¹, S. Antonucci⁴, B. Nisini⁴, C. Dougados⁵, and M. Takami⁶

¹ INAF-Osservatorio Astrofisico di Arcetri, Largo E. Fermi 5, I-50125 Firenze, Italy
e-mail: lindapod@arcetri.astro.it, fran@arcetri.astro.it

² Centro de Astrofísica da Universidade do Porto, Rua das Estrelas s/n, P-4150-762 Porto, Portugal
e-mail: pgarcia@astro.up.pt

³ Departamento de Engenharia Física, Faculdade de Engenharia da Universidade do Porto, Portugal

⁴ INAF-Osservatorio Astronomico di Roma, Via di Frascati 33, I-00040 Monte Porzio Catone, Italy
e-mail: nisini@mporzio.astro.it, antoniucci@mporzio.astro.it

⁵ Laboratoire d'Astrophysique de Grenoble, BP 53, 38041 Grenoble Cedex, France
e-mail: dougados@obs.ujf-grenoble.fr

⁶ Institute of Astronomy and Astrophysics, Academia Sinica, P.O. Box 23-141, Taipei 10617, Taiwan, R.O.C.
e-mail: hiro@asiaa.sinica.edu.tw

ABSTRACT

Context. Most of the observed emission lines and continuum excess from young accreting low mass stars (Classical T Tauri stars – CTTSs) take place in the star-disk or inner disk region. These regions have a complex emission topology still largely unknown.

Aims. In this paper the magnetospheric accretion and inner wind contributions to the observed permitted He and H near infrared (NIR) lines of the bright southern CTTS RU Lupi are investigated for the first time.

Methods. Previous optical observations of RU Lupi showed a large H α profile, due to the emission from a wind in the line wings, and a micro-jet detected in forbidden lines. We extend this analysis to NIR lines through seeing-limited high spectral resolution spectra taken with VLT/ISAAC, and adaptive optics (AO) aided narrow-band imaging and low spectral resolution spectroscopy with VLT/NACO. Using spectro-astrometric analysis we investigate the presence of extended emission down to very low spatial scales (a few AU).

Results. The He I λ 10830 line presents a P Cygni profile whose absorption feature indicates the presence of an inner stellar wind. Moreover the spectro-astrometric analysis evidences the presence of an extended emission superimposed to the absorption feature and likely coming from the micro-jet detected in the optical. On the contrary, the origin of the Hydrogen Paschen and Brackett lines is difficult to address. We tried tentatively to explain the observed line profiles and flux ratios with both accretion and wind models showing the limits of both approaches. The lack of spectro-astrometric signal indicates that the HI emission is either compact or symmetric. Our analysis confirms the sensitivity of the He I line to the presence of faint extended emission regions in the close proximity of the star.

Key words. stars: individual: RU Lupi – stars: winds, outflows – accretion, accretion disks – line: formation – techniques: high angular resolution

1. Introduction

Classical T Tauri stars (CTTSs) are young solar and lower mass stars presenting a rich emission line spectrum in excess of the continuum from the stellar photosphere. This emission includes Hydrogen lines, low energy forbidden lines and Helium lines together with a continuum excess – the veiling.

Optically and NIR forbidden emission lines, such as the [O I], [S II] and [Fe II] lines, have emission regions large enough to be resolved and are typically associated with outflowing jets (e.g. Bacciotti et al., 2000; Dougados et al., 2000; Pyo et al., 2006). On the other hand, the atomic permitted lines, such as the Hydrogen lines, are more difficult to interpret. The energy released by the accretion of matter onto the star can power the permitted line emission that is believed to arise from magnetospheric accretion columns and/or accretion shocks (e.g.

Muzerolle et al., 2001; Bouvier et al., 2007). The fact that the emission component of permitted atomic lines is attributed to infalling gas is supported by the presence of inverse P Cygni profiles, and by the correlation of their luminosities with the accretion luminosity, derived from the veiling (Muzerolle et al., 1998b,c). On the other hand, the blueshifted absorption features, when present, are an indicator of high velocity inner winds (e.g. Edwards et al., 1987; Najita et al., 2000). Indeed, several recent spectroscopic studies suggest that the emission of the permitted HI and He lines can actually include a contribution from both inflowing and outflowing gas (e.g. Beristain et al., 2001; Folha & Emerson, 2001; Takami et al., 2001; Whelan et al., 2004; Edwards et al., 2006). This has motivated hybrid models where the Hydrogen emission is due to both the magnetospheric accretion and a wind (Alencar et al., 2005; Kurosawa et al., 2006).

The fact that the collimated, spatially resolved jets, traced at large distance from the source by optical, near-infrared forbidden lines, are generated in circumstellar regions (less than 10 AU from the source) is predicted by theoretical models

Send offprint requests to: L. Podio

[★] Based on observations collected at the European Southern Observatory, Chile (ESO Programme 71.C-0703).

(Anderson et al., 2003; Ferreira et al., 2006) and observationally proved by the frequent detection of blueshifted absorption features in a number of strong permitted lines ($H\alpha$, Na, D, CaII, MgII, Najita et al. 2000), formed close to the star. Signatures of outflowing gas revealed by absorption features can also be searched in the profile of the HeI $\lambda 10830$ line (Takami et al., 2002; Edwards et al., 2003; Dupree et al., 2005). Edwards et al. (2006) analysed a sample of 31 T Tauri stars and showed that the HeI line is much more sensitive than the usually used $H\alpha$ line to trace inner winds in absorption (in 71% of the sources was detected an absorption feature in the HeI line against only 10% of detections in the $H\alpha$ line). Beristain et al. (2001) showed that the diagnostic power of permitted Helium lines in tracing inner winds, lies in their high excitation potential (20-50 eV), that restricts the line formation to a region of either high temperature or close proximity to a source of ionising radiation.

In order to investigate the reliability of such scenarios, we have observed the circumstellar region of the T Tauri star RU Lupi in the NIR wavelength range.

This source is one of the most active and well known T Tauri stars (Lamzin et al., 1996; Stempels & Piskunov, 2002; Herczeg et al., 2005) and it is a good target to investigate the inner winds and accretion flows down to very small spatial scales. RU Lupi is located at a distance of only 140 pc (de Zeeuw et al., 1999), allowing us to reach small spatial scales with high angular resolution instrumentation and/or specialised techniques of data analysis. In particular, NACO at the VLT was used to take high angular resolution images and low spectral resolution spectra. With VLT/ISAAC seeing limited and high spectral resolution spectra were obtained. A spectro-astrometric analysis was applied. Spectro-astrometry is a powerful technique to obtain positional information on the region originating the emission in the components of a line profile even in seeing-limited conditions. Takami et al. (2001), for example, using spectro-astrometry, found that the blueshifted and redshifted wings of the $H\alpha$ line emitted by RU Lupi show a spatially symmetric offsets with respect to the source, in the same direction of the jet traced, on higher spatial scales, by the forbidden [O I] and [S II] lines. Whelan et al. (2004) detected a similar extended emission in the wings of the Pa β line in three T Tauri sources (DG Tau, V536 Aql, and LkH α 321).

In this paper we present the results obtained from such a study and, in particular, a detailed analysis about the origin of the Paschen and Brackett HI lines and the HeI $\lambda 10830$ line. The paper is structured as follows: in Sect. 2 we present the different set of observations and the data reduction process; in Sect. 3 the observed line profiles and fluxes are analysed; moreover we present the concepts underlying the spectro-astrometry technique and the obtained position spectra; finally in Sect. 4 we discuss the origin of permitted H and He lines by means of a model for wind and accretion, and of the results obtained with spectro-astrometry. In the Conclusions (Sect. 5) we summarize our findings.

2. Observations & Data Reduction

Observations of RU Lupi were carried out in between April and June 2003 at the ESO Very Large Telescope. The first set of spectra was acquired at the UT4-YEPUN telescope using the infrared camera and spectrometer CONICA, working in cascade to the adaptive optics (AO) system NAOS, and the 86 mas width slit. The AO system allows one to obtain a high spatial resolution of $\sim 0''.08$ - $0''.12$ (full width at half maximum - FWHM

- of a point source), sampled by a pixel scale of $0''.054$. The second set of data was taken at the UT1-ANTU telescope using ISAAC with the $0''.3$ slit to obtain a high spectral resolution ($R \sim 10000$; spectral sampling: $\sim 14 \text{ km s}^{-1}$; pixel scale: $0''.147/\text{pixel}$), while the spatial resolution is limited by the seeing (FWHM $\sim 0''.6$ - $0''.8$). The NACO observations cover all the J and H bands wavelength ranges ($R \sim 400$ and $R \sim 1500$ respectively) while the ISAAC spectra centered at 1.08, 1.27 and $1.588 \mu\text{m}$ cover very short wavelength segments. Both the NACO and the ISAAC spectra were obtained at two slit position angles (217° and 127°), i.e. parallel and perpendicular to the jet direction as determined by Takami et al. (2001).

In addition two sets of images of the source in the narrow band filters centered around the HeI $\lambda 10830$ and [FeII] $\lambda 1.25, 1.64 \mu\text{m}$ lines, and around their near continuum (at 1.09, 1.24 and $1.75 \mu\text{m}$), were taken with NAOS/CONICA.

The information about the spectral observations and the images are summarized in Tab.1.

The spectra were reduced using standard IRAF tasks and Eclipse routines from the ESO pipeline. The images were corrected for bad pixels and cosmic rays and for ghosts, then flat-fielded, and sky-subtracted. Wavelength calibration was performed using the spectra of the arc lamps for the NACO data and the sky OH lines for the ISAAC spectra. The systemic motion of the object was subtracted using the radial velocity in the local standard of rest frame, determined by Takami et al. (2001) through the Li $\lambda 6707.815$ absorption line on the stellar atmosphere, $V_{LSR} = 8 \pm 2 \text{ km s}^{-1}$. The spectra were corrected for the atmospheric transmission and for the efficiency of the camera, and then flux calibrated using a telluric spectro-photometric standard. The typical uncertainty for the flux calibration is of $\sim 5\%$. Since the observed telluric stars are of type B, the absorption HI lines were subtracted before the correction. Unfortunately the Br10, Br13 and Br15 absorption lines were deeply blended with the atmospheric features in the telluric spectra. In the NACO spectra, because of the low resolution, it was not possible to perform a de-blending and subtract these HI absorption lines in the spectrum of the telluric. Thus the fluxes and the equivalent widths of the Br10, Br13 and Br15 lines measured from the NACO spectra are only upper limits. In the ISAAC telluric spectra, on the contrary, the HI lines were de-blended from the atmospheric features and subtracted. Even at the higher spectral resolution of the ISAAC data, however, this process is not very accurate and implies an oversubtraction. For this reason the fluxes, the FWHM and the equivalent widths of the Br10, Br13 and Br15 lines inferred from the ISAAC spectra should be considered as lower limits.

The NACO images were reduced using standard procedures: removal of bad pixel and cosmic rays, dark subtraction, flat-fielding and sky-subtraction. Then the images acquired with the narrow band filters centered on the continuum emission were subtracted from the images filtered on the line emission (HeI and [Fe II]). The subtraction was performed by: (i) choosing images with similar PSF, to minimize the effects of a different distribution of the emission in the different filters; (ii) normalizing the images for the source flux estimated through a gaussian bidimensional fit.

3. Results

Analysis of the NACO imaging data showed that no physical companion is detected in the continuum frames in the limit of our spatial resolution ($\sim 14 \text{ AU}$). No extended emission structure

Table 1. Instrumental setup during observations

Instrument	"/pix	Slit	Date	λ (μm)	R	PA	$T_{int} \times N_{ex}$
NACO imaging	0.013	n.a.	20/25-5-03	NB 1.08, 1.09	n.a.	n.a.	$10.8\text{s} \times 12$
				NB 1.24, 1.26			$9\text{s} \times 12$
				NB 1.64, 1.75			$9\text{s} \times 12$
NACO spectroscopy	0.054	$0''.086 \times 40''$	16-6-2003	J: 0.91-1.37	400	$217^\circ, 127^\circ$	$18\text{s} \times 10$
				H: 1.50-1.84	1500		
ISAAC	0.147	$0''.3 \times 120''$	26-6-2003	SZ: 1.06-1.1	11500	$217^\circ, 127^\circ$	$300\text{s} \times 4$
				J: 1.24-1.3	10500	$217^\circ, 127^\circ$	$300\text{s} \times 4$
				H: 1.54-1.62	10000	217°	$250\text{s} \times 2$

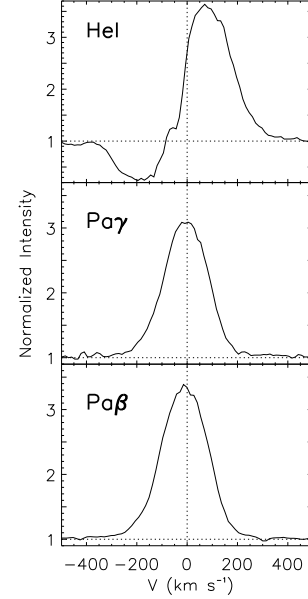
is detected in continuum subtracted emission line frames at HeI and [Fe II] $\lambda\lambda 1.25, 1.64 \mu\text{m}$. This constrains the presence of wind emission in the HeI and [Fe II] lines over a region smaller than 14 AU.

The NACO low resolution spectra show strong hydrogen recombination lines in emission (Br10 to Br19 and Pa β , Pa γ) and the HeI 1.0830 μm line (see Fig.1 and Tab. 2). The ISAAC medium spectral resolution spectra allow us to study in more detail the spectral profiles of the HeI, Pa β , Pa γ and Br 13, 14, 15, 16 lines (see Fig.2 and Tab. 3), as well as their spatial displacement with respect to the continuum emission through spectroastrometry (see Sect. 3.3). No [Fe II] lines are detected at 1.25, 1.32, 1.53, 1.60 and 1.64 μm both in the NACO and in the ISAAC spectra. The lack of [Fe II] emission is not expected in this source. In fact, studies of HH jets in the optical and in the NIR range (Podio et al., 2006) showed that optical jets emit also in the NIR [Fe II] lines, unless the density in the jet beam is very low ($n_e < 10^3 \text{ cm}^{-3}$). In RU Lupi, indeed, on one hand strong and spatially extended emission in the optical forbidden lines ([S II], [O I], and [N II]) was observed by Takami et al. (2001); on the other hand, electron densities higher than 10^4 - 10^5 cm^{-3} were estimated by the same authors based on the [S II] lines equivalent width ratio. Therefore, iron lines should be present in the spectra. Possible reasons for the non detection of Fe emission could be the fact that a short integration time was used, or that a strong depletion of iron caused an emission fainter than the predicted one. In fact, an increase of depletion near to the source has been observed in other jet sources as, e.g. HH 1 (Nisini et al., 2005).

Table 2. Equivalent widths (EW) and dereddened line fluxes (F) from NACO spectroscopy.

λ μm	Line	EW km s^{-1}	F $10^{-13} \text{ erg s}^{-1} \text{ cm}^{-2}$
1.0830	HeI	452	40 ± 5
1.0941	Pa γ	457	40 ± 5
1.2822	Pa β	434	32 ± 3
1.5265	Br 19	9	0.5 ± 0.2
1.5346	Br 18	14	0.8 ± 0.2
1.5443	Br 17	20	1.1 ± 0.2
1.5561	Br 16	19	1.1 ± 0.1
1.5705	Br 15	46	$2.7 \pm 0.3^*$
1.5885	Br 14	31	1.8 ± 0.2
1.6114	Br 13	55	$3.1 \pm 0.3^*$
1.6412	Br 12	48	2.7 ± 0.3
1.6811	Br 11	63	3.5 ± 0.3
1.7367	Br 10	78	$3.9 \pm 0.3^*$

* The equivalent widths (EW) and the fluxes (F) of the Br10, Br13 and Br15 line are only upper limits to the real flux, due to the presence of HI lines blended with atmospheric features in the spectrum of the telluric standard (see Sect. 2).

**Fig. 2.** ISAAC spectra of the HeI $\lambda 10830$, Pa γ and Pa β lines. The lines are normalized to the continuum intensity.**Table 3.** Line properties from ISAAC spectroscopy.

λ μm	Line	V_{peak} km s^{-1}	ΔV km s^{-1}	EW km s^{-1}	F^a $10^{-13} \text{ erg s}^{-1} \text{ cm}^{-2}$
^b 1.0830	HeI ab	-200	-	133	-
^c 1.0830	HeI em	70	-	581	47 ± 6
1.0941	Pa γ	-5	206	475	40 ± 5
1.2822	Pa β	-11	214	562	38 ± 3
1.5561	Br 16	-31	179	23	1.2 ± 0.2
*1.5705	Br 15	-16	128	20	1.0 ± 0.2
1.5885	Br 14	-22	185	43	2.2 ± 0.2
*1.6114	Br 13	-19	159	44	2.7 ± 0.3

^a The fluxes (F) are corrected for dust extinction (see Sect 3.1).

^{b,c} Parameters relative to the absorption (ab) and emission (em) part of the HeI line profile (see Fig. 2).

* Due to the presence of HI lines blended with atmospheric features in the spectrum of the telluric standard, the parameters inferred for the Br13 and Br15 lines are only rough estimates (see Sect. 2). In particular the width, ΔV , and the flux, F, are lower limits.

3.1. HI emission lines.

The availability of complementary data sets (see Tab. 1) allows us to investigate the origin of HI lines through both the measured line fluxes and the line profiles. The characteristics and the parameters of the lines profiles can be retrieved from the ISAAC spectra thanks to the high spectral resolution. The centre (V_{peak}), the FWHM (ΔV), the equivalent width (EW), and

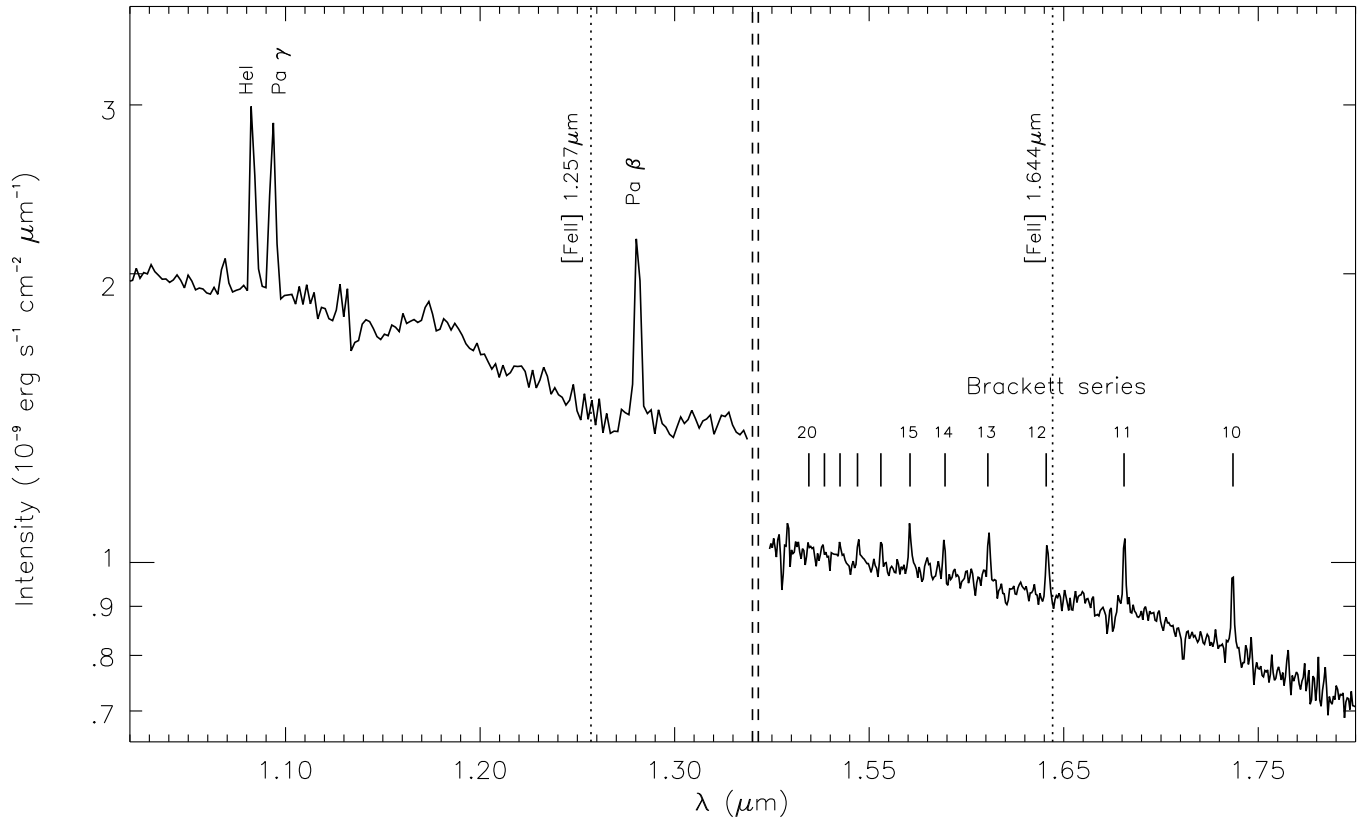


Fig. 1. Low resolution NACO spectrum of RU Lupi in the J and H bands. The HeI $\lambda 10830$ line and the HI emission lines from the Paschen and the Brackett series are shown. The dotted lines indicate the wavelength position of the [Fe II] lines at 1.25 and 1.64 μm , that were not detected in our spectra.

the dereddened flux (F) of the HI lines which are in the spectral range covered by the ISAAC spectra (Pa β , Pa γ and Br 13, 14, 15 and 16) are summarized in Tab. 3. The classification proposed by Reipurth et al. (1996) for the H α line profiles was already used for NIR Hydrogen lines by Folha & Emerson (2001) and Whelan et al. (2004). According to this classification scheme, the detected HI lines are type I profiles, i.e. they are nearly symmetric showing no evidence for absorption features, but they have large FWHM and extended wings. All the Paschen and Brackett lines detected, in fact, are broad ($\Delta V \sim 200$ km s $^{-1}$, except for the Br 13 and the Br 15 lines for which we get only a lower limit to the FWHM) and slightly blueshifted ($-5 < V_{\text{peak}} < -30$). In particular, the intensity profiles normalized to the continuum emission of the Pa γ and Pa β lines are shown in Figure 2. Both the Pa γ and Pa β lines have a broad nearly symmetric profile peaking at 3-3.5 times the intensity of the continuum. The profile is centered at -5 and -11 km s $^{-1}$, respectively, and extends at least from -300 km s $^{-1}$ to +200 km s $^{-1}$.

The ratios between the lines of the Paschen and Brackett series can be used to retrieve further informations about the origin of the HI lines. The NACO spectra have too low spectral resolution to derive the properties of the line profiles (V_{peak} , ΔV). They can be used, however, to measure the equivalent widths and the fluxes of the Paschen and Brackett lines (see Tab. 2). With respect to the ISAAC data, these spectra have the advantage of covering all the Brackett lines from the Br 10 up to the Br 19 in the same spectral segment, allowing us to measure and compare the fluxes of all the lines without introducing calibration problems. First, we corrected the observed fluxes for the reddening. We used the average value of the visual extinction

estimated by Giovannelli et al. (1995) in the circumstellar region of RU Lupi ($A_V = 0.7 \pm 0.3$) and the extinction law derived by Rieke & Lebofsky (1985). The dereddened line fluxes of the Paschen and the Brackett lines are summarized in Tab. 2 for the NACO data and in Tab. 3 for the ISAAC ones. The error affecting the line fluxes and their ratios is computed considering the noise over the continuum and the uncertainty on the A_V value. Then we computed the Brackett decrement, i.e. the ratios between the intensity of the Brackett lines coming from the upper level n and the first line of the series. The first Brackett line in the spectral range covered by our spectra is the Br 10, but this line is not well corrected for the atmospheric transmission (see Sect. 2). Thus we used the ratios with the Brackett 11 line. The Brackett ratios, $\text{Br}n/\text{Br}11$, as a function of the upper level n , are plotted in Fig. 3 (the ratios Br15/Br11 and Br13/Br11 are not taken into consideration since for the Br13 and Br15 lines we have only an upper limit of the flux, see Sect. 2). In the Figure we overplotted the theoretical values of the Brackett ratios calculated for two different cases: (i) the solid line traces the ratios in the case of optically thick emission at the temperature $T=10^4$ K (black-body emission); (ii) the four dotted lines correspond to Case B recombination (Hummer & Storey, 1987) for $T=10^4$ K and four different values of the electron density. Note that for the considered values of the electron density, variations of the temperature between 10^3 and 10^5 K leave the curves almost identical. The plot of Fig. 3 shows that the ratios between the Brackett lines are well fitted by case B recombination, i.e. by optically thin emission. As we will discuss in Sect. 4.1, however, case B cannot reproduce the observed fluxes for typical values of the emitting volume.

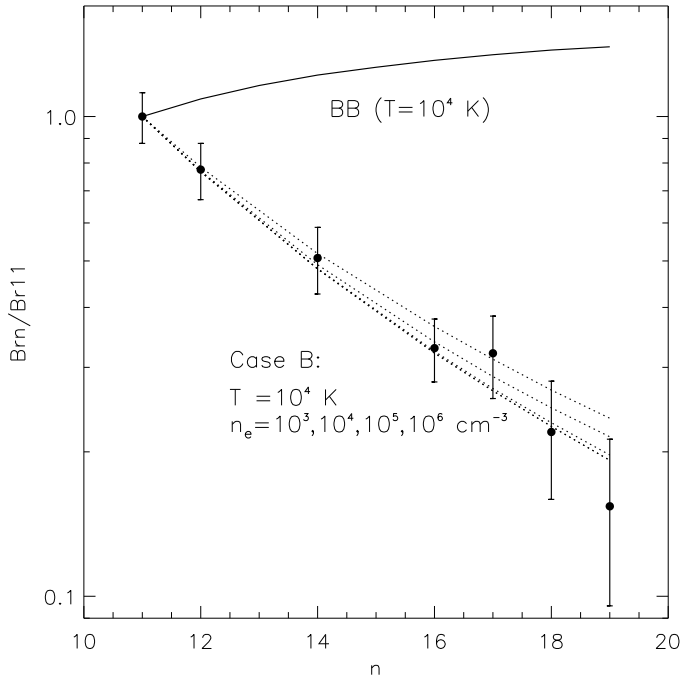


Fig. 3. Ratios of the Brackett lines with respect to Br11 versus the upper quantum number n . The solid line indicates the theoretical value of the ratios expected in case of optically thick emission at $T=10000$ K. The four dotted lines are the ratios expected from case B recombination (Hummer & Storey 1987) assuming $T=10000$ K and $n_e=10^3, 10^4, 10^5, 10^6$ cm^{-3} going from the lower to the upper line.

To avoid systematic errors that can affect the lines of the same series, and to constrain even more tightly the emission conditions, we considered also the ratio between the observed Paschen lines, $\text{Pa}\beta/\text{Pa}\gamma$. The measured $\text{Pa}\beta/\text{Pa}\gamma$ ratio retrieved from the NACO spectra is $\sim 0.8 \pm 0.1$, and the one retrieved from the ISAAC ones is $\sim 1 \pm 0.1$. Such values cannot be produced by the case B recombination. In fact, for any choice of the electron density and the temperature between 10^2 and 10^{10} cm^{-3} and $5 \cdot 10^2$ and $3 \cdot 10^4$ K, respectively, case B gives $\text{Pa}\beta/\text{Pa}\gamma > 1.4$. On the other hand, in the case of optically thick emission (blackbody emission) the $\text{Pa}\beta/\text{Pa}\gamma$ ratio is ~ 0.6 at $T=10^4$ K, and ~ 0.7 at $T=5 \cdot 10^3$ K. This implies that the Paschen lines are not reproduced by one of these limiting cases and that their ratio strongly depends from their relative optical depth.

3.2. The HeI $\lambda 10830$ line.

The HeI line profile obtained from medium resolution ISAAC spectra (Fig. 2) shows a typical P-Cygni profile with the emission part peaking at $+70$ km s^{-1} , and extending up to at least $+430$ km s^{-1} , and a broad blueshifted absorption penetrating up to 80% of the continuum at $V \sim 200$ km s^{-1} and ranging from -360 km s^{-1} to -90 km s^{-1} (see Tab. 3). The absorption feature clearly indicates the presence of an inner wind (Edwards et al., 2003). The efficiency of the HeI $\lambda 10830$ transition in tracing outflowing gas is due to the “metastability” of its lower level ($2s^3S$). Even if energetically far above the singlet ground state (21 eV), this level is radiatively isolated from it and collisionally de-excitation is very low. This means that, once it is populated, via photoionisation followed by recombination and cascade and/or via collisional excitation from the ground state, this

level becomes easily over-populated. The absorption feature is generated mainly via resonant scattering since the $\lambda 10830$ transition is the only permitted radiative transition from its upper state to a lower one and the electron density is unlikely high enough to cause collisional excitation or de-excitation. Edwards et al. (2003, 2006) demonstrate that the shape and width of the HeI $\lambda 10830$ line can constrain the wind launch region. They show that a broad and deep blue absorption, as the one detected in our spectra, require formation in a wind emerging radially from the star rather than from the disk. In fact, the broad range of velocities covered by the absorption feature can be explained by radially emerging wind streamlines absorbing the $1 \mu\text{m}$ continuum from the stellar surface, thus tracing the full acceleration region of the inner wind. On the contrary, a disk- or x- wind is confined to nearly parallel streamlines emerging at an angle to the disk surface and thus the continuum photons from the star will intercept a narrower range of velocities giving rise to narrow absorption feature as the ones shown in Edwards et al. (2006). In conclusion, the absorption feature in our spectra appears to indicate the presence of an inner wind radially emerging from the star. Further insight on the geometry and the presence of different wind contributions to the HeI $\lambda 10830$ line can be retrieved from the spectro-astrometric analysis presented in Sect. 3.3 and discussed in Sect. 4.2.

The emission part of the line, instead, is produced by the accreting gas columns and, partially, by the resonant scattering process. The contribution from the latter depends on the electron density and in our case should be much lower than the loss of flux in the absorption part of the line. In fact, the detection of the absorption feature indicates that the efficiency of collisional de-excitation is much lower with respect to the radiative decay.

3.3. Spectro-astrometry

Further to the standard spectroscopic analysis, we performed a spectro-astrometric analysis of the data. Following this procedure the displacement of the emission centroid of the lines with respect to the source continuum is determined (e.g., Bailey, 1998). This means that one can detect extended emission in a line beyond the seeing limit, down to (sub-)AU scales. On the other hand, the technique is sensitive only to asymmetric emission and, since it measures a barycentre, it gives only a lower limit to the size of the emission region. The technique consists in accurately measuring the trace of each A-B spectrum by Gaussian fitting the spectrum spatial profile at each wavelength. In this way one recovers the wavelength dependent centroid (i.e. the so called “position spectrum”) and gaussian FWHM of the spectra. The residual FWHM, obtained subtracting the FWHM of the continuum emission, can be sensitive to differential size variations in the emission region. Examples of the application of spectro-astrometry can be found in Takami et al. (2001), Whelan et al. (2005).

The essential requirements for this kind of analysis are a good spectral and spatial sampling, and a high signal-to-noise ratio (SNR). Thus we applied spectro-astrometry only to the ISAAC spectra, in which the lines are very well resolved ($\text{SNR} \sim 100$) and well sampled spectrally ($\Delta V \sim 200$ km s^{-1} , spectral sampling ~ 14 km s^{-1}), while the spatial sampling is moderately good ($\text{FWHM} \sim 0''.6-0''.8$, spatial sampling: $0''.147$). Since the trace of the star is tilted in the ISAAC spectrograph, the centroid is corrected for this distortion with a polynomial fit. The typical spectro-astrometric error is given by the accuracy in measuring the centroid of the spatial profile through the gaussian fit

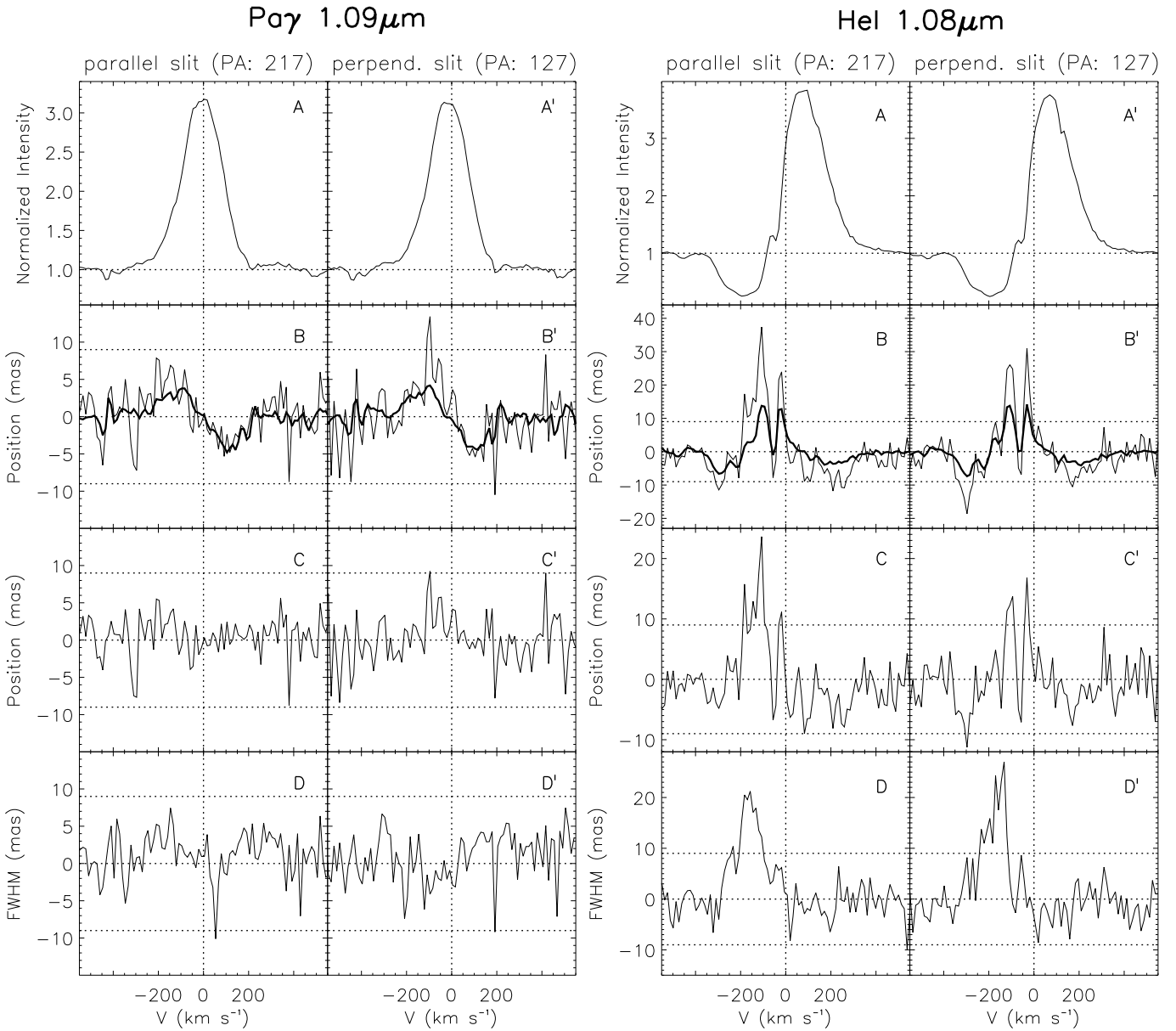


Fig. 4. ISAAC spectroscopy of RU Lupi Pay (left) and HeI (right), with the slit parallel to the jet and perpendicular. The line profiles normalized to the continuum emission are presented in the upper panels – A and A'. The spectro-astrometric signal is presented in the second panels – B and B'. The overplotted solid line is the spectro-astrometric signal due to a distorted PSF caused by tracking error or unstable active optics. The signal is simulated following the procedure of Brannigan et al. (2006) (see text). The residual signal obtained subtracting the simulated signal to the detected one is shown in the third panels – C and C'. Finally, the residual FWHM of the gaussian fit is presented in the lower panels – D and D'. The vertical dotted lines show the zero velocity of the line. The horizontal dotted lines indicate the continuum emission level and the $\pm 3\sigma$ threshold due to the signal-to-noise.

and is equal to $\sigma \sim 0.5 \text{ FWHM} / \sqrt{N_{ph}}$ (Takami et al., 2003). For the considered lines ($N_{ph} > 10^5$), this accuracy turns out to be ~ 1 mas. In the case of the He line, however, the signal is fainter in the absorption part ($N_{ph} \sim 10^4 - 10^5$). Therefore, we adopted $\sigma \sim 3$ mas, which is the average value of the error across the line profile. Moreover, since the spatial sampling for the ISAAC data is not exceptional, we used a conservative value of the threshold of 3σ (see Fig. 4). We checked the position spectra for the presence of artifacts following the procedure of Brannigan et al. (2006). These authors showed that the distortion of the PSF caused by tracking errors of the telescope or unstable active optics during an exposure, can induce artificial signals. These instrumen-

tal biases can be simulated in shape and magnitude calculating the spectro-astrometric signal obtained from a modeled distorted PSF. We used the same procedure than in Brannigan et al. (2006) to simulate the biases that can be produced with our instrumental setting (cf. Tab. 1). The shape of the artifacts produced by a distorted PSF depends on the slope of the line profile. In particular, the peaks of the simulated biases appear at velocities where the gradient of the line profile is the largest. This explain the double peak of the simulated spectro-astrometric signal in the blueshifted part of the HeI line (see panel B and B' of Fig. 4). The magnitude of such biases, instead, depends on the amplitude of the distortion of the PSF with respect to the slit axis, i.e. on the parameters Δx_1 , Δx_2 , Δy_1 , Δy_2 in Eq. (4) of Brannigan et al.

(2006). The maximum biases are obtained when the distortion of the PSF in the slit is maximum, i.e. when we put in Eq. (4) of Brannigan et al. (2006) $\Delta x_1 = \Delta x_2 = 0''.15$, $\Delta y_1 = \Delta y_2 = 0''.15$, so that the total slit illumination displacement (Δy) is equal to the slit width, $0''.3$. The resulting spurious signal was then subtracted from the position spectra.

The position spectra obtained for the Pa β and Brackett lines do not show any shift of the centroid with respect to the continuum emission. On the other hand, in the Pa γ and the HeI line we found a spectro-astrometric signal (see Fig. 4). In panels A and A' the intensity spectrum of the two lines in the two slit positions is shown. The position spectrum, in panels B and B', indicate a shift of the centroid of the emission with respect to the continuum emission both in the parallel and in the perpendicular slit. The superimposed solid line is the spurious spectro-astrometric signal that can be induced by an elongated PSF in the slit in the worst possible case. In panel C and C' the residual signal obtained subtracting the determined biases is shown. Finally in panels D and D' we plot the residual FWHM of the gaussian fit.

Fig. 4 shows that there is no real signal in the Pa γ line. In fact, there is no residual in the position spectra of this line after the subtraction of the biases as well as in the spatial FWHM across the profile. In the HeI line, on the contrary, the position spectra cleaned by artifacts (panels C and C') show a shift over the signal-to-noise limit (9 mas, corresponding to ~ 1.3 AU) in the blueshifted part of the line. The residual FWHM across the profile presents a significant signal in the same velocity range where the spectro-astrometric signal is detected ($-50 \text{ km s}^{-1} < V < -200 \text{ km s}^{-1}$), reaching differential sizes of $0''.025$. A broader FWHM is expected in the region where the absorption feature is detected, because the continuum emission is much fainter. It is, however, interesting to notice that: (i) the spatial profile can be identified very well over the background noise across the entire HeI spectral profile (the signal-to-noise ratio is $S/N \sim 100$ in the spectral region covered by the absorption feature and ~ 10 times higher in the emission part of the line); (ii) the broadening of the line is not symmetric with respect to the peak of the absorption feature ($V_{\text{peak}} \sim -200 \text{ km s}^{-1}$). Instead, a constant or increasing FWHM in the parallel and perpendicular slit respectively, is measured in the region where the spectro-astrometric signal is detected ($-200 \text{ km s}^{-1} < V < -100 \text{ km s}^{-1}$). This suggests that multiple spatial components are contributing to the line profile in such region of the ‘‘P Cygni’’ absorption feature. The interpretation of the detected spectro-astrometric signal is discussed in Sect. 4.2.

4. Discussion

As illustrated in the Introduction the excitation mechanism of the HI lines is an actively debated topic. Up to a few years ago, both the observations and the models focused on the Balmer lines, and in particular on the H α line. The large amount of optical observations evidenced the limits of both the accretion and the wind models in reproducing the Balmer lines and motivated the development of hybrid models with more complex geometries (e.g., Kurosawa et al., 2006). On the other hand, the capacity of these models to reproduce the profiles and fluxes of the HI infrared lines was poorly tested. Interestingly, the observations of Paschen and Brackett lines, such as the ones presented in Folha & Emerson (2001), Nisini et al. (2004), Whelan et al. (2004), Edwards et al. (2006), have shown that the magnetospheric accretion models cannot fully reproduce the characteristics of the observed profiles, in favour again of an hybrid wind/accretion model.

As we have shown in the previous section, the Paschen and the Brackett lines in our spectra present blue-shifted broad symmetric profiles ($V_{\text{peak}} \sim -17 \text{ km s}^{-1}$ and $\Delta V \sim 200 \text{ km s}^{-1}$). These are difficult to reproduce if one adopts *separately* a wind model or, alternatively, a magnetospheric accretion model. Wind models generally predict red-shifted peaks and strongly asymmetric profiles with P-Cygni absorption features, as the one detected in the HeI line (Calvet et al., 1992). Hartmann et al. (1990) were able to reproduce more symmetric Br γ and Br α profiles, without the P-Cygni absorption feature with a model of magnetically driven wind, but their peaks are still red-shifted. Edwards et al. (1987) showed that an optically thick circumstellar disk may cause the occultation of the red-shifted part of the profile thus explaining blue-shifted peaks. In any case, asymmetric profiles are expected.

On the other hand, magnetospheric accretion models (Muzerolle et al., 1998a) predict blue-shifted peaks, but asymmetric and narrow profiles ($\Delta V \sim 100 \text{ km s}^{-1}$) often showing inverse P-Cygni absorption. Muzerolle et al. (2001) retrieved from their accretion model more symmetric and broad line profiles, taking into account line damping due to different broadening mechanisms, but this effect is really important only for H α and Balmer lines, while it is negligible for Paschen and Brackett lines.

We will now examine how the above scenarios fit in the case of our RU Lupi spectra.

4.1. Accretion vs wind

As illustrated in Sect. 3.1 the case B recombination well reproduces the Brackett decrement, but not the Pa β /Pa γ ratio, whose value implies that these two lines are optically thick. Moreover, case B recombination assumes (i) a constant density, which is not applicable to the circumstellar region of T Tauri stars, and (ii) optically thin lines. To reproduce the observed fluxes, however, the latter hypothesis would imply an emitting volume corresponding to a spherical envelope extending up to 40 AU from the source, which is unrealistic according to the models of circumstellar accretion/ejection structure (e.g., Nisini et al., 2004). To investigate the origin of the HI lines one has to assume a variable density profile, and the optical depth and the flux of the Paschen and Brackett lines will be retrieved integrating along the line of sight.

Nisini et al. (2004) analysed the Brackett lines in the Class I source HH 100 IR, finding line profiles very similar to the ones of our Paschen and Brackett lines. Interestingly, they found that the Brackett decrement in HH 100 IR is neither reproduced by the Case B recombination curves (i.e. optically thin emission), nor by the blackbody emission (i.e. completely thick emission). The authors suggested that these lines are emitted in an expanding envelope of ionised Hydrogen, and thus different lines are tracing different layers of the envelope according to their optical depth. Following this idea they were able to reproduce the ratios between the optically thick Brackett lines through a simple model of spherical wind.

We used the same approach to reproduce the Br n /Br l ratios (Fig. 3), the Pa β /Pa γ ratio and the observed line fluxes both in the accretion and in the wind hypothesis adopting a toy model consisting in a spherical envelope of ionised Hydrogen, extending from an inner radius r_i to an outer radius r_{out} , where LTE conditions are assumed. If the envelope is expanding (wind hypothesis) or infalling (accretion hypothesis) the radiation transfer can be treated in the Sobolev approximation following the formalism described in Castor (1970) and Nisini et al. (1995). The gas can

be only partially ionised, and, therefore, the envelope total mass loss or accretion rate is $\dot{M}_{wind/accr} = \dot{M}_{ion}/x_e$, where x_e is the ionisation fraction. The electron density in the envelope is given by the continuity equation, $n_e = \dot{M}_{wind/accr} x_e / 4\pi m_H r^2 V(r)$.

Using this model both the wind and the accretion hypothesis can be tested just changing the velocity law $V(r)$. In fact, this will imply a different density profile and thus a difference in the relative optical depths of the lines in the two cases.

In the wind hypothesis the HI envelope is expanding and the gas velocity follows a general law of the type $V(r) = V_0 + (V_{max} - V_0)(1 - (r_i/r)^\alpha)$, i.e. the gas is accelerated from an initial velocity at the base of the wind, V_0 , at the maximum velocity V_{max} at a distance that depends on the parameter α (Nisini et al., 2004). V_{max} is the maximum velocity of the expanding gas. The FWHM of the observed lines is determined by the velocity of the gas particles, thus we retrieve from the observed profiles $V_{max} \sim 200 \text{ km s}^{-1}$.

The simulated emission is tuned by a proper choice of the input parameters. For typical values of the size of the envelope ($r_i = 1 R_*$, $r_{out} = 3 - 10 R_*$) and of the electron temperature ($T = 10^4 \text{ K}$), and taking $\alpha=4$ and $V_0=30 \text{ km s}^{-1}$ as in Nisini et al. (2004), we are able to reproduce the Brn/Br11 ratios and the absolute fluxes of the Paschen and almost all the Brackett lines (within $\pm 4\sigma$) for $\dot{M}_{ion} \sim 2 \cdot 10^{-8} M_\odot \text{ yr}^{-1}$. On the other hand, in this way we are not able to reproduce the observed Pa β /Pay ratio (Pa β /Pay $\sim 1.3-1.4$). Considering a slower acceleration of the wind ($\alpha=1-3$) and/or a lower temperature (T down to $5 \cdot 10^3 \text{ K}$) the Pa β /Pay ratio decreases to $\sim 1-1.3$ and the absolute fluxes are in agreement with the observed ones but the Brackett ratios are not reproduced because the lines optical depths are too large. Taking lower values of the mass loss rate ($\dot{M}_{ion} < 10^{-8} M_\odot \text{ yr}^{-1}$), that is the fundamental parameter regulating the emission in the HI lines, we obtain a good fit of the Brackett decrement for r_{out} within $3 - 10 R_*$ and values of the exponent in the acceleration law of the wind between 1 and 4. The absolute fluxes, however, are too low in this case (3-4 times smaller than the observed ones) and the Pa β /Pay ratio is > 1.4 . To obtain the required Pa β /Pay one should assume a value of \dot{M}_{ion} higher than $2 \cdot 10^{-8} M_\odot \text{ yr}^{-1}$. For such a massive wind, however, the Brackett decrement and line fluxes would no longer be fitted by the model because their optical depth would be too large.

Since we could not find a choice of the parameters for the wind model reproducing at the same time the Brackett decrement and the observed Pa β /Pay ratio, we tentatively tried to use the model to simulate the emission from a spherical accreting envelope, by reversing the sign of the gas speed. A spherical model is not the best approximation of the accretion process, that, according to the most recent models, proceeds along the magnetic field lines, in an axisymmetric non-spherical geometry (Hartmann et al., 1994; Muzerolle et al., 1998a). Nevertheless, we have adopted the spherical model as a first approximation, in order to check if the observed ratios are better reproduced by accretion rather than by an outflow.

If we assume that the HI lines are mainly excited in the accretion columns we can derive an estimate of the mass accretion rate from the luminosity of the Pa β line. To this aim, we use the empirical relation between $L(\text{Pa}\beta)$ and the accretion luminosity derived by Muzerolle et al. (1998c) and Natta et al. (2002):

$$\log L_{acc}/L_\odot = 1.36 \log L(\text{Pa}\beta)/L_\odot + 4. \quad (1)$$

The mass accretion rate is then computed from L_{acc} as $\dot{M}_{acc} = L_{acc} R_*/(GM_*)$. Using for RU Lupi $M_* = 0.8 M_\odot$ and $R_* = 1.6 R_\odot$ (Lamzin et al., 1996; Herczeg et al., 2005), we obtain $\dot{M}_{acc} = 2 \cdot 10^{-7} M_\odot \text{ yr}^{-1}$. This value is in agreement with previous

estimates of Lamzin et al. (1996), that tuned the value of \dot{M}_{acc} in order to reproduce through their model the observed continuum energy distribution (see, however, Herczeg et al. 2005, for an alternative derivation of \dot{M}_{acc} using the accretion luminosity estimated from the UV excess).

In the case of an accreting envelope the typical velocity law is $V(r) = V_{max} r^{-0.5}$. We fixed the size of the envelope and the temperature ($r_i = R_*$, $r_{out} = 3R_*$, $T=10^4 \text{ K}$), and examined the results obtained varying the ionisation fraction x_e , and thus the electron density of the accreting columns for $\dot{M}_{acc} = 2 \cdot 10^{-7} M_\odot \text{ yr}^{-1}$. If the gas is fully ionised ($x_e=1$) we obtain Pa β /Pay ~ 0.7 , but the Brackett decrement is not reproduced, because the optical depth of these lines is too large, and the absolute fluxes of all the lines are higher than the observed one by one order of magnitude. Indeed, estimates of the ionisation fraction for different values of the temperature and the mass loss rate show that the gas is only partially ionised in the circumstellar envelope (e.g., Natta et al., 1988). Assuming $x_e=0.4$ both the Brackett decrement and the ratio between the Paschen lines are well reproduced, but the absolute fluxes are still too high by a factor 3-4. To obtain absolute fluxes in agreement with the observed ones we have to assume low ionisation fractions, down to $x_e=0.15$. In this case, however, we are not able to reproduce the Pa β /Pay ratio. We note that in a non-spherical geometry the lines become optically thick for lower mass accretion rates, and thus both a “thick” Pa β /Pay ratio and lower absolute fluxes can be obtained at the same time. In such a model, however, the profiles of the HI lines are predicted to be much narrower than the observed ones, i.e. FWHMs of the order of 100 km s^{-1} would be obtained, in contrast with our observations.

In conclusion, our analysis shows that neither a spherically symmetric wind nor spherically symmetric accretion can reproduce the Brackett and Paschen line ratios and fluxes. There are a few recent observational results suggesting that both the emission from the accretion columns and from a wind may contribute to the line profiles. Takami et al. (2001) and Whelan et al. (2004), for example, found that the gas from a wind contributes to the emission in the wings of their H α and Pa β lines, thus producing line profiles broader than the ones predicted by magnetospheric accretion models. In our case, however, the observed H lines do not show the core/wings structure which is expected when both the accreting material and a wind are contributing to the emission.

To investigate further the possibility of a co-existence of emission from both inflowing and outflowing gas in our H lines we analysed critically the spectro-astrometric results as described below.

4.2. Insights from spectro-astrometry

In the last two Sections we showed that both the accretion model and the wind model fail in reproducing all the characteristic of the observed NIR HI lines. A powerful technique to investigate the origin of the HI emission and separate the accretion and the wind contributions to the line profiles is spectro-astrometry (see, e.g., Takami et al., 2001; Whelan et al., 2004, 2005). In fact, outflowing gas presents an extended emission testified by a detectable positional shift, while accreting gas remain concentrated on the source location.

Although Takami et al. (2001) detected extended emission in the wings of the H α line up to $\sim 3 \text{ AU}$ from RU Lupi, we found that there is no spectro-astrometric signal in the HI NIR lines (see Fig. 4). The lack of signal indicates that: (i) either the emission comes from a compact region (smaller than $\sim 1.3 \text{ AU}$); (ii)

or, if there is a further emission from an extended region, this is symmetric, thus not detectable through spectro-astrometry, or too faint with respect to the emission from the star and the accretion columns (see below).

On the contrary, we do detect after subtraction of possible biases a substantial spectro-astrometric signal in the HeI $\lambda 10830$ line (Fig. 4, panels C, C'). The shift found in the HeI line is interpreted as an emission originating in the base of the jet, that partially fills the absorption feature of the "P Cygni" profile due to the inner wind. The inner stellar wind acts like a natural coronagraph hiding the star along the blueshifted absorption, increasing the contrast of emission from outer regions. This could explain why we detect a positional shift in the HeI line and not in the NIR HI lines. A similar extended emission superimposed to the blueshifted absorption feature of the HeI line was found by Takami et al. (2002) in DG Tauri. Following the same reasoning of Takami et al. (2002) we suggest that there are three contributors to the profile of the HeI line: (i) red-shifted emission presumably due to accreting gas; (ii) blue-shifted absorption due to the presence of an inner spherical wind emerging from the stellar surface; (iii) blue-shifted extended emission between $V \sim 50$ km s⁻¹ and $V \sim 200$ km s⁻¹ superimposed to the absorption feature and coming from a jet at a larger distance from the source. This emission is supposed to come from the base of the collimated micro-jet detected by Takami et al. (2001) in the forbidden [S II] and [O I] lines and in the H α line. The velocity range covered by the HeI extended component is the same as in the H α line. The HeI spectro-astrometric signal extends up to ~ 20 mas from the source (~ 3 AU). However, as explained in Sect. 3.3, this is only a lower limit to the true angular scale of the emission region which could be more extended.

Combining in a bi-dimensional plane the shifts detected along the parallel and the perpendicular slits we find that the extended emission is not completely aligned with the jet of Takami et al. (2001), the misalignment being not greater than 30°. This may be justified by the fact that: (i) the jet may be not well collimated in the He line; (ii) our observations were made 4 years later and a 200 km s⁻¹ stream moves 1 AU in a week. Furthermore, Takami et al. (2001) do observe variability in their spectro-astrometric data taken several years apart. Another discrepancy with respect to the result obtained by Takami et al. (2001) in the H α line is that we did not detect extended emission in the red-shifted part of the HeI line. This can be due, again, to the fact that the jet emission in the HI and HeI lines is fainter than in the optical H α line and it can be evidenced by spectro-astrometry only over the blueshifted absorption, which hides the emission from the star and increases the contrast of outer emission.

5. Conclusions

In this paper we analysed infrared spectra and images of the T Tauri star RU Lupi, in order to find observational constraints for the physics of the circumstellar region. This source was previously observed in the optical wavelength range by other authors, that reported about a strong accretion activity and the presence of a micro-jet detected in the optical forbidden lines and in the H α line (Takami et al., 2001). We have observed for the first time RU Lupi in the NIR with high angular and spectral resolution. In this paper we report about these observations and, in particular, we investigate the origin of the permitted H and He NIR lines through the analysis of the line profiles and fluxes, and using the spectro-astrometry technique which allows us to constrain

the emission region of each velocity component of the detected lines.

The problem of the origin of HI lines was widely debated in the last decades. Many different models were proposed to reproduce their profiles and fluxes: wind models (e.g., Hartmann et al., 1990), accretion models (e.g., Hartmann et al., 1994; Muzerolle et al., 1998a, 2001) and also hybrid models accounting for the emission from both the accretion columns and the wind (e.g., Kurosawa et al., 2006). These analyses, however, focused mainly on Balmer lines observed in the optical range. The Paschen and Brackett lines detected in our NIR spectra of RU Lupi present broad, slightly blueshifted and nearly symmetric profiles, which are difficult to reproduce with either a wind or an accretion model. This was already noted, in general, by Folha & Emerson (2001), Whelan et al. (2004), Nisini et al. (2004). We tentatively used a toy model of a spherical envelope of partially ionised Hydrogen with a wind or an accretion velocity profile (Nisini et al., 2004) to constrain the HI line ratios and fluxes. This analysis showed that neither a spherical wind nor spherical accretion can reproduce the Brackett and Paschen decrement and fluxes.

Our spectro-astrometric analysis did not highlight any extended emission in the Paschen and Brackett lines, suggesting that the region emitting the HI NIR lines is very compact (< 1.3 AU) and/or symmetric. On the other hand, the HeI $\lambda 10830$ line blueshifted absorption feature clearly indicates the presence of an inner wind. The wide range of velocities covered by the absorption feature favours the geometry of a spherical wind emerging from the stellar surface rather than a disk wind as found in many TTS by Edwards et al. (2006). In addition, the spectro-astrometric analysis highlighted the presence of an emission superimposed to the absorption feature that extends up to at least ~ 3 AU from the source and covers the same velocity range of the H α extended emission found by Takami et al. (2001). We suggest that this emission comes from the blue lobe of the micro-jet detected in the optical lines by Takami et al. (2001). Interestingly, the HeI showed to be more sensitive than the HI NIR lines to faint extended emission because the absorption feature increases the contrast between the emission from the extended region and the continuum from the source. This confirms the potential of the HeI $\lambda 10830$ line to investigate the complex geometry of the inner part of the circumstellar region of CTTS, where both the accretion and the ejection processes take place (see also Edwards et al., 2006). On the base of these results, future high angular resolution observations of the permitted H and He lines in CTTS can give useful hints to the understanding of the accretion/ejection mechanisms and the development of theoretical models accounting for the emission from both the outflowing and the accreting gas.

Acknowledgements. Linda Podio thanks CAUP for hospitality during the development of this work. We are also grateful to the referee, Dr. Suzan Edwards, for the attentive comments which allowed us to improve the first version of this paper. This work was partially supported by the European Community's Marie Curie Research and Training Network JETSET (Jet Simulations, Experiments and Theory) under contract MRTN-CT-2004-005592, and by the Consiglio Nazionale delle Ricerche in the framework of a CNR/GRICES Agreement. P.J.V.G. work was supported in part by the Fundação para a Ciência e a Tecnologia through projects POCI/CTE-AST/55691/2004 and PTDC/CTE-AST/65971/2006 from POCTI, with funds from the European program FEDER.

References

- Alencar, S. H. P., Basri, G., Hartmann, L., & Calvet, N. 2005, *A&A*, 440, 595
- Anderson, J. M., Li, Z.-Y., Krasnopolsky, R., & Blandford, R. D. 2003, *ApJ*, 590, L107

- Bacciotti, F., Mundt, R., Ray, T. P., Eislöffel, J., Solf, J., & Camezind, M. 2000, *ApJ*, 537, L49
- Bailey, J. 1998, *MNRAS*, 301, 161
- Beristain, G., Edwards, S., & Kwan, J. 2001, *ApJ*, 551, 1037
- Bouvier, J., Alencar, S. H. P., Harries, T. J., Johns-Krull, C. M., & Romanova, M. M. 2007, *Protostars and Planets V*, 479
- Brannigan, E., Takami, M., Chrysostomou, A., & Bailey, J. 2006, *MNRAS*, 367, 315
- Calvet, N., Hartmann, L., & Hewett, R. 1992, *ApJ*, 386, 229
- Castor, J. I. 1970, *MNRAS*, 149, 111
- de Zeeuw, P. T., Hoogerwerf, R., de Bruijne, J. H. J., Brown, A. G. A., & Blaauw, A. 1999, *AJ*, 117, 354
- Dougados, C., Cabrit, S., Lavalley, C., & Ménard, F. 2000, *A&A*, 357, L61
- Dupree, A. K., Brickhouse, N. S., Smith, G. H., & Strader, J. 2005, *ApJ*, 625, L131
- Edwards, S., Cabrit, S., Strom, S. E., Heyer, I., Strom, K. M., & Anderson, E. 1987, *ApJ*, 321, 473
- Edwards, S., Fischer, W., Kwan, J., Hillenbrand, L., & Dupree, A. K. 2003, *ApJ*, 599, L41
- Edwards, S., Fischer, W., Hillenbrand, L., & Kwan, J. 2006, *ApJ*, 646, 319
- Ferreira, J., Dougados, C., & Cabrit, S. 2006, *A&A*, 453, 785
- Folha, D. F. M., & Emerson, J. P. 2001, *A&A*, 365, 90
- Giovanelli, F., Vittone, A. A., Rossi, C., Errico, L., Bisnovatyi-Kogan, G. S., Kurt, V. G., Lamzin, S. A., Larionov, M., Sheffer, E. K., Sidorenkov, V. N. 1995, *A&AS*, 114, 341G
- Hartmann, L., Avrett, E. H., Loeser, R., & Calvet, N. 1990, *ApJ*, 349, 168
- Hartmann, L., Hewett, R., & Calvet, N. 1994, *ApJ*, 426, 669
- Herczeg, G. J., et al. 2005, *AJ*, 129, 2777
- Hummer, D. G., & Storey, P. J. 1987, *MNRAS*, 224, 801
- Kurosawa, R., Harries, T. J., & Symington, N. H. 2006, *MNRAS*, 370, 580
- Lamzin, S. A., Bisnovatyi-Kogan, G. S., Errico, L., Giovanelli, F., Katysheva, N. A., Rossi, C., & Vittone, A. A. 1996, *A&A*, 306, 877
- Muzerolle, J., Calvet, N., & Hartmann, L. 1998a, *ApJ*, 492, 743
- Muzerolle, J., Hartmann, L., & Calvet, N. 1998b, *AJ*, 116, 455
- Muzerolle, J., Hartmann, L., & Calvet, N. 1998c, *AJ*, 116, 2965
- Muzerolle, J., Calvet, N., & Hartmann, L. 2001, *ApJ*, 550, 944
- Najita, J. R., Edwards, S., Basri, G., & Carr, J. 2000, *Protostars and Planets IV*, 457
- Natta, A., Giovanardi, C., & Palla, F. 1988, *ApJ*, 332, 921
- Natta, A., Testi, L., Comerón, F., Oliva, E., D'Antona, F., Baffa, C., Comoretto, G., & Gennari, S. 2002, *A&A*, 393, 597
- Nisini, B., Milillo, A., Saraceno, P., & Vitali, F. 1995, *A&A*, 302, 169
- Nisini, B., Antonucci, S., & Giannini, T. 2004, *A&A*, 421, 187
- Nisini, B., Bacciotti, F., Giannini, T., Massi, F., Eislöffel, J., Podio, L., & Ray, T. P. 2005, *A&A*, 441, 159
- Podio, L., Bacciotti, F., Nisini, B., Eislöffel, J., Massi, F., Giannini, T., & Ray, T. P. 2006, *A&A*, 456, 189
- Pyo, T.-S., et al. 2006, *ApJ*, 649, 836
- Reipurth, B., Pedrosa, A., & Lago, M. T. V. T. 1996, *A&AS*, 120, 229
- Rieke, G. H., & Lebofsky, M. J. 1985, *ApJ*, 288, 618
- Stempels, H. C., & Piskunov, N. 2002, *A&A*, 391, 595
- Takami, M., Bailey, J., Gledhill, T. M., Chrysostomou, A., & Hough, J. H. 2001, *MNRAS*, 323, 177
- Takami, M., Chrysostomou, A., Bailey, J., Gledhill, T. M., Tamura, M., & Terada, H. 2002, *ApJ*, 568, L53
- Takami, M., Bailey, J., & Chrysostomou, A. 2003, *A&A*, 397, 675
- Whelan, E. T., Ray, T. P., & Davis, C. J. 2004, *A&A*, 417, 247
- Whelan, E. T., Ray, T. P., Bacciotti, F., Natta, A., Testi, L., & Randich, S. 2005, *Nature*, 435, 652